BOUNDARY LAYER EFFECTS OF INTERLAMINAR STRESSES ADJACENT TO A HOLE IN A LAMINATED COMPOSITE PLATE

E. S. FOLIAS

Department of Mechanical Engineering, University of Utah, Salt Lake City, UT 84112, U.S.A.

Abstract—An eigenfunction expansion is developed for the determination of the three-dimensional stress field in the neighborhood of the intersection of the free edge of a hole and an interface in a laminated composite plate. For transversely isotropic laminae, the stress field is shown to possess a weak singularity whose strength depends on the material constants, the fiber orientations of the two adjacent laminae as well as the polar angle θ. Results for [0°/90°], [0°/70°], [0°/45°], and [0°/20°] are presented and the best and worst fiber orientations are identified.

Finally, the interlaminar stresses are computed and the variation as a function of the angle θ is identified. The circumferential stress $\sigma_{\theta\theta}$ is shown to possess a small jump across the interface. Results for its behavior in the interior of each layer are also given.

1. INTRODUCTION

Despite careful design, practically every structure contains stress concentrations due to holes. Bolt holes and rivet holes are necessary components for structural joints. It is not surprising, therefore, that the majority of service cracks nucleate in the vicinity of a hole. While the subject of stress concentrations is certainly familiar to engineers, the situation is significantly more complex in the case of high-performance laminated composite materials. The presence of a hole in the laminate introduces significant stress contributions in the third dimension which create a very complicated three-dimensional (3-D) stress field in the vicinity of the hole. Moreover, this complex state of stress may depend on the stacking sequence of the laminate, the fiber orientation of each lamina as well as the material properties of the fiber and of the matrix. Ultimately, these stress concentrations form a primary source of damage initiation and property degradation, particularly in the presence of cyclic loadings. Recent experimental investigations carried out by Bakis and Stinchcomb (1986) on graphite–epoxy laminates which have been weakened by a circular hole give us a better insight of this damage growth development under the action of cyclic loadings. In general, the progression of this damaged process may be characterized as (i) debonding along fiber–matrix interfaces, (ii) matrix cracking parallel to the fibers, (iii) matrix cracking between fibers, (iv) delamination along the interface of two adjacent laminae with different fiber orientations, and (v) fiber breakage.

Thus, if rational designs using fiber-reinforced–resin matrix composite laminates are to be made, their performance under static, dynamic, fatigue and environmental loads need to be predictable. The first step towards this goal is the realization that the ultimate failure, as well as many other aspects of the composite behavior, is the result of the growth and accumulation of microdamage to the fibers, matrix and their interfaces. Thus, it appears that any generally successful model of performance and failure must incorporate the effects of this damage in some way. This certainly represents a challenge. In this paper, we will address only one form of such damage, that of delamination.

Delamination has long been recognized as one of the most important failure modes in laminated composite structures. The growth of a delamination may result in a substantial reduction of strength and stiffness of the laminate. The identification, therefore, of such locations in a composite structure is of great interest to the designer. Experimental studies by Pipes *et al.* (1973) have shown that the delamination mode of failure is most likely to initiate at the free edges. One conjectures, therefore, that the stresses at the intersection
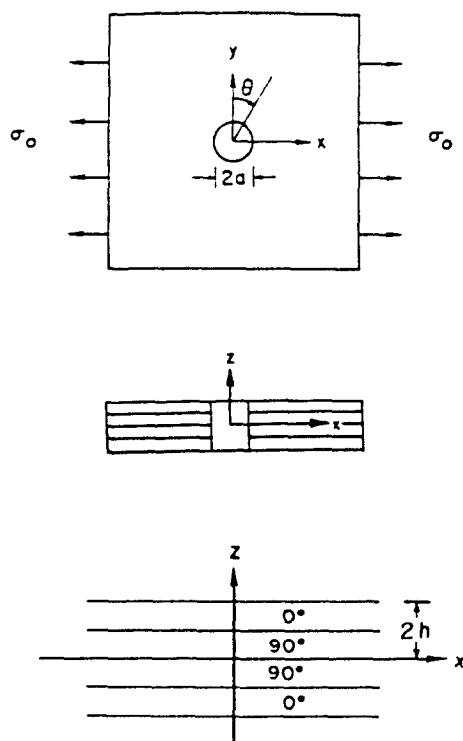
Fig. 1. Laminated plate of arbitrary thickness with a circular hole.

between a free edge and an interface may well be singular. Indeed, recent analytical investigations (Wang and Choi, 1982; Zwiers *et al.*, 1982) on straight free edges show that a stress singularity exists there for certain types of laminates.

Alternatively, a curved free edge is inherently a 3-D problem which presents greater mathematical difficulties. For this reason, past analyses have been based primarily on finite element methods with standard finite elements (Raju and Grews, 1982), as well as elements which incorporate the stress singularity in the formulation (Rybicki and Schmueser, 1978; Ericson *et al.*, 1984). While such methods can provide us with stress trends in the boundary layer region, it is rather difficult to extract from them with certainty the order of the prevailing stress singularity which is present at the material interface. Moreover, experimental investigations carried out on straight edges by Pagano (1974) show that the laminate stacking sequence can effect the static strength of the laminates. Similar experimental observations were also made by Daniel *et al.* (1974) on plates with circular holes. The subject, therefore, does warrant further investigation.

Recently, Folias (1988) investigated analytically the interlaminar stresses at the boundary layer of a hole free-edge, but for two isotropic materials of different material constants. The analysis showed that the stress field there possesses a weak† singularity, which singularity depends only on the material properties. In this paper, the author extends this analysis to include also transversely isotropic laminae with a [0/90], [0/45] as well as other stacking sequences.

2. FORMULATION OF THE PROBLEM

Consider the equilibrium of a laminated composite plate which occupies the space $|x| < \infty$, $|y| < \infty$ and $|z| \leqslant 2h$ and contains a cylindrical hole of radius a whose generators are perpendicular to the bounding planes, namely $z = \pm 2h$. The plate consists of laminae made of transversely isotropic material with a 0/90/0 stacking sequence. Let the plate be subjected to a uniform tensile load σ_0 along the y-axis and parallel to the bounding planes (see Fig. 1).

† Less than 0.33.

In the absence of body forces, the coupled differential equations governing the displacement functions u, v and w are

$$C_{11}\frac{\partial^2 u}{\partial x^2} + C_{66}\frac{\partial^2 u}{\partial y^2} + C_{55}\frac{\partial^2 u}{\partial z^2} + (C_{12}+C_{66})\frac{\partial^2 v}{\partial x \partial y} + (C_{13}+C_{55})\frac{\partial^2 w}{\partial x \partial z} = 0 \qquad (1)$$

$$(C_{21}+C_{66})\frac{\partial^2 u}{\partial x \partial y} + C_{66}\frac{\partial^2 v}{\partial x^2} + C_{22}\frac{\partial^2 v}{\partial y^2} + C_{44}\frac{\partial^2 v}{\partial z^2} + (C_{23}+C_{44})\frac{\partial^2 w}{\partial y \partial z} = 0 \qquad (2)$$

$$(C_{31}+C_{55})\frac{\partial^2 u}{\partial x \partial z} + (C_{32}+C_{44})\frac{\partial^2 v}{\partial x \partial z} + C_{55}\frac{\partial^2 w}{\partial x^2} + C_{44}\frac{\partial^2 w}{\partial y^2} + C_{33}\frac{\partial^2 x}{\partial z^2} = 0, \qquad (3)$$

where the C_{ij} terms are the material constants defining a layer which has its fibers running parallel to the x-axis. For the next layer, the fibers will be running parallel to the y-axis and the governing equations will be obtained from the above by simply interchanging the appropriate coordinates.

The stress–displacement relations for the layer are given by the constitutive relations

$$\begin{bmatrix} \sigma_{xx} \\ \sigma_{yy} \\ \sigma_{zz} \\ \tau_{yz} \\ \tau_{xz} \\ \tau_{xy} \end{bmatrix} = \begin{bmatrix} C_{11} & C_{12} & C_{13} & 0 & 0 & 0 \\ C_{21} & C_{22} & C_{23} & 0 & 0 & 0 \\ C_{31} & C_{32} & C_{33} & 0 & 0 & 0 \\ 0 & 0 & 0 & C_{44} & 0 & 0 \\ 0 & 0 & 0 & 0 & C_{55} & 0 \\ 0 & 0 & 0 & 0 & 0 & C_{66} \end{bmatrix} \begin{bmatrix} e_{xx} \\ e_{yy} \\ e_{zz} \\ 2e_{yz} \\ 2e_{xz} \\ 2e_{xy} \end{bmatrix}. \qquad (4)$$

As to boundary conditions, we require that:

$$\text{at} \quad z = \pm 2h: \quad \text{the surface stresses must vanish} \qquad (5)$$

$$\text{at} \quad z = \pm h: \quad \text{the displacements and surface stresses must match} \qquad (6)$$

$$\text{at} \quad r = a: \quad \text{the surface stresses must vanish.} \qquad (7)$$

Finally, in order to complete the formulation of the problem, the loading conditions far away from the hole must be satisfied.

3. ASYMPTOTIC SOLUTION AT THE INTERFACE

The main objective of this analysis is to derive an asymptotic solution for the 3-D stress field in the immediate vicinity of the region where the interface between two laminae meets the free-of-stress surface of the hole. Thus, guided by a general analytical solution for the equilibrium of a linear elastic isotropic layer which Folias and Reuter (1990) and Folias and Wang (1990) have recently constructed, we assume the complementary displacement field to be of the form†

(i) for lamina [0]

$$u^{(1)} = \sin \theta \left\{ l_{11}\frac{\partial^2}{\partial(r-a)^2} + l_{12}\frac{\partial^2}{\partial(h-z)^2} \right\} \frac{\partial^3 H}{\partial(r-a)\partial(h-z)^2} \qquad (8)$$

† The angle θ is defined in Fig. 1.

$$v^{(1)} = \cos\theta \left\{ l_{21} \frac{\partial^2}{\partial(r-a)^2} + l_{22} \frac{\partial^2}{\partial(h-z)^2} \right\} \frac{\partial^3 H}{\partial(r-a)\partial(h-z)^2} \tag{9}$$

$$w^{(1)} = \left\{ l_{31} \frac{\partial^4}{\partial(r-a)^4} + l_{32} \frac{\partial^4}{\partial(r-a)^2\partial(h-z)^2} + l_{33} \frac{\partial^4}{\partial(h-z)^4} \right\} \frac{\partial H}{\partial(h-z)} \tag{10}$$

where

$$l_{11} = -(C_{13}+C_{55})[C_{66}\sin^2\theta + C_{22}\cos^2\theta] + (C_{12}+C_{66})(C_{23}+C_{44})\cos^2\theta \tag{11}$$

$$l_{12} = -(C_{13}+C_{55})C_{44} \tag{12}$$

$$l_{21} = (C_{13}+C_{55})(C_{21}+C_{66})\sin^2\theta - (C_{23}+C_{44})(C_{11}\sin^2\theta + C_{66}\cos^2\theta) \tag{13}$$

$$l_{22} = -(C_{23}+C_{44})C_{55} \tag{14}$$

$$l_{31} = (C_{11}\sin^2\theta + C_{66}\cos^2\theta)(C_{66}\sin^2\theta + C_{22}\cos^2\theta) - \tfrac{1}{4}(C_{12}+C_{66})^2\sin^2(2\theta) \tag{15}$$

$$l_{32} = C_{44}(C_{11}\sin^2\theta + C_{66}\cos^2\theta) + C_{55}(C_{66}\sin^2\theta + C_{22}\cos^2\theta) \tag{16}$$

$$l_{33} = C_{44}C_{55}. \tag{17}$$

In writing the above displacements, we used a cylindrical coordinate system (see Fig. 1) and, furthermore, assumed that $(r-a) \ll a$. In view of the above, one, by direct substitution, can show† that the governing equations (1)–(3) are indeed satisfied provided the unknown function H satisfies the differential relation

$$\left[\frac{\partial^2}{\partial(r-a)^2} + c_1 \frac{\partial^2}{\partial(h-z)^2} \right]\left[\frac{\partial^2}{\partial(r-a)^2} + c_2 \frac{\partial^2}{\partial(h-z)^2} \right] \cdot \left[\frac{\partial^2}{\partial(r-a)^2} + c_3 \frac{\partial^2}{\partial(h-z)^2} \right] H = 0, \tag{18}$$

where the c_1, c_2 and c_3 are functions of C_{ij} and θ, and represent the roots of the cubic equation

$$c^3 - \frac{T_2}{T_1}c^2 + \frac{T_3}{T_1}c - \frac{T_4}{T_1} = 0, \tag{19}$$

with

$$T_1 = (C_{11}\sin^2\theta + C_{66}\cos^2\theta)(C_{66}\sin^2\theta + C_{22}\cos^2\theta)(C_{55}\sin^2\theta + C_{44}\cos^2\theta)$$
$$- \tfrac{1}{4}(C_{12}+C_{66})^2(C_{55}\sin^2\theta + C_{44}\cos^2\theta)\sin^2(2\theta) \tag{20}$$

$$T_2 = (C_{11}\sin^2\theta + C_{66}\cos^2\theta)[C_{33}(C_{66}\sin^2\theta + C_{22}\cos^2\theta)$$
$$+ C_{44}(C_{55}\sin^2\theta + C_{44}\cos^2\theta) - (C_{23}+C_{44})^2\cos^2\theta]$$
$$+ (C_{12}+C_{66})[2(C_{23}+C_{44})(C_{31}+C_{55})\sin^2\theta - (C_{21}+C_{66})C_{33}\sin^2\theta]\cos^2\theta$$
$$- (C_{13}+C_{55})^2(C_{66}\sin^2\theta + C_{22}\cos^2\theta)\sin^2\theta$$
$$+ C_{55}(C_{66}\sin^2\theta + C_{22}\cos^2\theta)(C_{55}\sin^2\theta + C_{44}\cos^2\theta) \tag{21}$$

---

† Write first the governing equations in cylindrical coordinates and then use the assumption. See Appendix A.

$$T_3 = C_{55}[C_{33}(C_{66}\sin^2\theta + C_{22}\cos^2\theta) + C_{44}(C_{55}\sin^2\theta + C_{44}\cos^2\theta)$$

$$-(C_{23}+C_{44})^2\cos^2\theta] - (C_{13}+C_{55})^2 C_{44}\sin^2\theta + [C_{11}\sin^2\theta + C_{66}\cos^2\theta]C_{33}C_{44} \quad (22)$$

$$T_4 = C_{33}C_{44}C_{55}. \quad (23)$$

(ii) for lamina [90°]

$$u^{(2)} = \sin\theta\left\{\tilde{I}_{11}\frac{\partial^2}{\partial(r-a)^2} + \tilde{I}_{12}\frac{\partial^2}{\partial(h-z)^2}\right\}\frac{\partial^3\tilde{H}}{\partial(r-a)\partial(h-z)^2} \quad (24)$$

$$v^{(2)} = \cos\theta\left\{\tilde{I}_{21}\frac{\partial^2}{\partial(r-a)^2} + \tilde{I}_{22}\frac{\partial^2}{\partial(h-z)^2}\right\}\frac{\partial^3\tilde{H}}{\partial(r-a)\partial(h-z)^2} \quad (25)$$

$$w^{(2)} = \left\{\tilde{I}_{31}\frac{\partial^4}{\partial(r-a)^4} + \tilde{I}_{32}\frac{\partial^4}{\partial(r-a)^2\partial(h-z)^2} + \tilde{I}_{33}\frac{\partial^4}{\partial(h-z)^4}\right\}\frac{\partial\tilde{H}}{\partial(h-z)} \quad (26)$$

$$\tilde{I}_{11} = -(C_{23}+C_{44})[C_{66}\sin^2\theta + C_{11}\cos^2\theta] + (C_{12}+C_{66})(C_{13}+C_{55})\cos^2\theta \quad (27)$$

$$\tilde{I}_{12} = -(C_{23}+C_{44})C_{55} \quad (28)$$

$$\tilde{I}_{21} = \{(C_{23}+C_{44})(C_{21}+C_{66})\sin^2\theta - (C_{13}+C_{55})(C_{22}\sin^2\theta + C_{66}\cos^2\theta)\} \quad (29)$$

$$\tilde{I}_{22} = -(C_{13}+C_{55})C_{44} \quad (30)$$

$$\tilde{I}_{31} = (C_{22}\sin^2\theta + C_{66}\cos^2\theta)(C_{66}\sin^2\theta + C_{11}\cos^2\theta) - (C_{12}+C_{66})^2\sin^2\theta\cos^2\theta \quad (31)$$

$$\tilde{I}_{32} = C_{55}(C_{22}\sin^2\theta + C_{66}\cos^2\theta) + C_{44}(C_{66}\sin^2\theta + C_{11}\cos^2\theta) \quad (32)$$

$$\tilde{I}_{33} = C_{44}C_{55}, \quad (33)$$

and the function $\tilde{H}(r-a, h-z)$ is of the same form as the H of layer [0''], except that c_1, c_2, c_3 are now replaced by the appropriate $\tilde{c}_1, \tilde{c}_2, \tilde{c}_3$ of layer [90°]. It remains, therefore, for us to construct a solution to eqn (18). To accomplish this, we introduce the local, to the corner, stretched coordinate system (see Fig. 2), i.e.

$$r-a = \rho\cos\phi \quad (34)$$

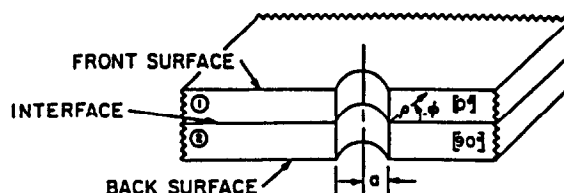$$\frac{(h-z)}{\sqrt{c_1}} = \rho\sin\phi. \quad (35)$$

Fig. 2. Definition of local coordinates at the interface.

Omitting the long and tedious mathematical details, the solution to equation (18), in terms of the local coordinates, is found to be†

$$H(\rho, \phi) = \rho^{\chi}\left\{A_1 \cos(\chi\phi) + B_1 \sin(\chi\phi) + \frac{1}{\chi}\int_0^{\phi} \psi_1(\xi)\sin[\chi(\phi - \xi)]\,d\xi\right\} + (\rho^{\chi+1}) \quad (36)$$

where

$$\psi_1(\phi) = \left\{A_2 \cos[(\chi - 2)\tan^{-1}(\phi_2)] + B_2 \sin[(\chi - 2)\tan^{-1}(\phi_2)]\right.$$

$$\left. + \frac{1}{(\chi - 2)}\int_0^{\phi_2}\psi_2(\xi)\sin[(\chi - 2)(\phi_2 - \xi)]\,d\xi\right\}\left(\frac{\rho_2}{\rho}\right)^{\chi-2}, \quad (37)$$

$$\frac{\rho_2}{\rho} = \frac{\sqrt{1 + \frac{c_1}{c_2}\tan^2\phi}}{\sqrt{1 + \tan^2\phi}}, \quad (38)$$

$$\psi_2(\phi_2) = \left(\frac{\rho_1}{\rho_2}\right)^{\chi-4}\left\{A_1 \cos\left[(\chi - 4)\tan^{-1}\left(\sqrt{\frac{c_2}{c_1}}\tan\phi_2\right)\right]\right.$$

$$\left. + B_1 \sin\left[(\chi - 4)\tan^{-1}\left(\sqrt{\frac{c_2}{c_1}}\tan\phi_2\right)\right]\right\}, \quad (39)$$

$$\left(\frac{\rho_1}{\rho_2}\right) = \sqrt{\frac{1 + \frac{c_2}{c_1}\tan^2\phi_2}{1 + \tan^2\phi_2}} \quad (40)$$

$$\phi_2 = \tan^{-1}\left(\sqrt{\frac{c_1}{c_2}}\tan\phi\right). \quad (41)$$

and χ, A_i and B_i ($i = 1, 2, 3$) are constants to be determined from the boundary conditions.

Substituting the previously constructed displacement field into the boundary conditions:

at $\phi = 0$:

$$u^{(1)} = u^{(2)} \quad (42)$$

$$v^{(1)} = v^{(2)} \quad (43)$$

$$w^{(1)} = w^{(2)} \quad (44)$$

$$\sigma_{zz}^{(1)} = \sigma_{zz}^{(2)} \quad (45)$$

$$\tau_{xz}^{(1)} = \tau_{xz}^{(2)} \quad (46)$$

$$\tau_{yz}^{(1)} = \tau_{yz}^{(2)} \quad (47)$$

at $\phi = -(\pi/2)$:

$$\sigma_{rr}^{(1)} = 0 \quad (48)$$

† See Appendix A for details.

$$\tau_{r\theta}^{(1)} = 0 \tag{49}$$

$$\tau_{rz}^{(1)} = 0 \tag{50}$$

at $\phi = \pi/2$:

$$\sigma_{rr}^{(2)} = 0 \tag{51}$$

$$\tau_{r\theta}^{(2)} = 0 \tag{52}$$

$$\tau_{rz}^{(2)} = 0 \tag{53}$$

we arrive at a system of 12 algebraic equations, the determinant of which must vanish. This latter condition leads to the determination of the characteristic values α. In general, the values of α depend on the material constants C_{ij}, as well as on the angle θ.

4. THE ISOTROPIC CASE

As a limit check, we let the laminae be homogeneous and isotropic but of different material constants. Without going into the mathematical details, the material constants of lamina 1 become:

$$C_{11} = C_{22} = C_{33} = 2\left(\frac{1-v_1}{1-2v_1}\right)G_1 \tag{54}$$

$$C_{44} = C_{55} = C_{66} = G \tag{55}$$

$$C_{12} = C_{23} = C_{13} = \frac{2v_1}{1-2v_1}G_1, \tag{56}$$

in view of which the displacements reduce to:

$$u^{(1)} = \sin\theta \frac{\partial}{\partial(r-a)}\left\{\frac{G_1}{1-2v_1}\left[\frac{\partial^2}{\partial(r-a)^2} + \frac{\partial^2}{\partial(h-z)^2}\right]\right\}\frac{\partial^2 H}{\partial(h-z)^2} \tag{57}$$

$$v^{(1)} = \cos\theta \frac{\partial}{\partial(r-a)}\left\{\frac{G_1}{1-2v_1}\left[\frac{\partial^2}{\partial(r-a)^2} + \frac{\partial^2}{\partial(h-z)^2}\right]\right\}\frac{\partial^2 H}{\partial(h-z)^2} \tag{58}$$

$$w^{(1)} = G_1\left\{\frac{\partial^2}{\partial(r-a)^2} + \frac{\partial^2}{\partial(h-z)^2}\right\}\left\{2\left(\frac{1-v_1}{1-2v_1}\right)\frac{\partial^2 H}{\partial(r-a)^2} + \frac{\partial^2 H}{\partial(h-z)^2}\right\}. \tag{59}$$

Notice that the θ-dependence has totally been eliminated and that the function H now attains the very simple form

$$H = \rho^2\{A_1\cos(\alpha\phi) + B_1\sin(\alpha\phi) + A_2\cos(\alpha-2)\phi$$
$$+ B_2\sin(\alpha-2)\phi + A_3\cos(\alpha-4)\phi + B_3\sin(\alpha-4)\phi\} + (\rho^{\alpha+1}). \tag{60}$$

Similarly, the $\tilde{H}$ collapses to the same expression except that the constants A_i and B_i are replaced by $\tilde{A}_i$ and $\tilde{B}_i$, respectively. The numerical results for this case lead to the same
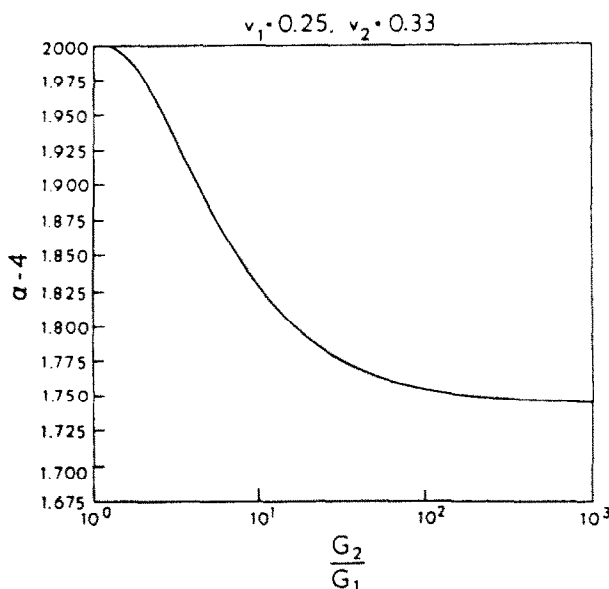
Fig. 3. Singularity strength for isotropic laminae.

results as those recently reported by Folias (1988). Figure 3, for example, depicts typical values of α.

5. CHARACTERIZATION OF THE FREE-EDGE STRESS SINGULARITY

Returning next to the algebraic system (42)–(53), if one considers the case of a graphite/epoxy layer, with coefficients C_{ij} (Knight, 1982):

$$C_{ij} = \begin{bmatrix} 20.6228 & 1.0381 & 1.0381 & 0.0000 & 0.0000 & 0.0000 \\ 1.0381 & 2.2301 & 1.2301 & 0.0000 & 0.0000 & 0.0000 \\ 1.0381 & 1.2301 & 2.2301 & 0.0000 & 0.0000 & 0.0000 \\ 0.0000 & 0.0000 & 0.0000 & 0.5000 & 0.0000 & 0.0000 \\ 0.0000 & 0.0000 & 0.0000 & 0.0000 & 0.8696 & 0.0000 \\ 0.0000 & 0.0000 & 0.0000 & 0.0000 & 0.0000 & 0.8696 \end{bmatrix}, \tag{61}$$

then the requirement of the determinant of the system to vanish leads to a transcendental equation for the roots α. The only roots of practical interest are those which lie in the interval $5 < \text{Re } \alpha < 6$. The numerical results for the 12×12 system were carried out in double precision. Omitting the long and tedious numerical details, the values of the characteristic α for [0 /90], [0 /70], [0 /45] and [0 /20] interfaces† are shown in Fig. 4. Two important characteristics are worth mentioning. First, the stress singularity is a function of the material constants C_{ij}, the angle of sweep θ and the fiber orientation of the respective laminae. Second, the singularity strength for anisotropic materials appears to be much weaker than that of isotropic materials. The latter may have severe consequences to the damage process and to the reduction of the overall strength in the plate. As a practical matter, if one plots the max $(\alpha - 6)$ as a function of the fiber angle orientation β for a $[0^\circ/\beta^\circ]$ interface one can identify the most and least desirable fiber orientations. This is depicted in Fig. 5.

Similar stress singularity profiles (see Fig. 4) have also been obtained by Wang and Choi (1982) in their pioneering work on straight edges using a different method of solution. The present analysis complements this and shows that, for sufficiently large holes, the results

† The results for the stresses are presently generalized for an arbitrary [0/β] interface.
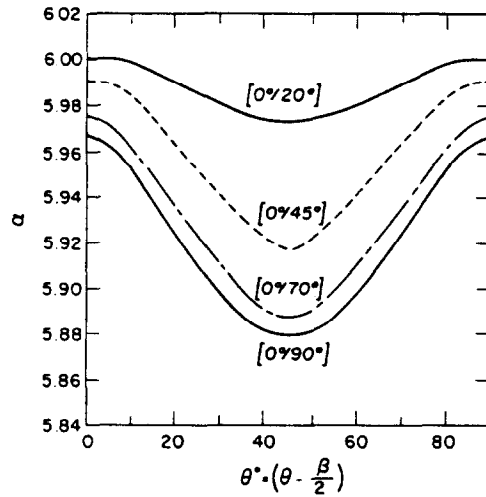
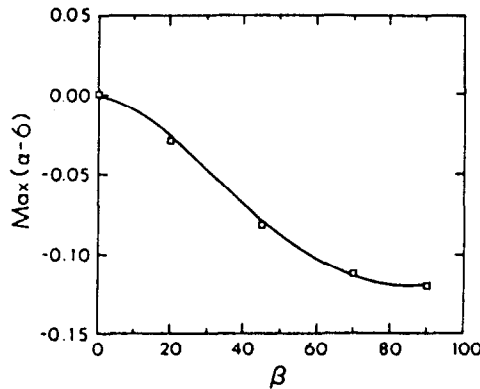Fig. 4. Singularity strength for transversely isotropic laminae [0/90].

Fig. 5. Best and worst fiber orientations.

for curved edges will be the same as those obtained near a straight free edge provided layer orientations in the second problem are properly chosen to reflect the circumferential position of a point on the hole boundary and the interface. While this result was to be expected, it could not be taken for granted. This is because the latter method represents a discrete, rather than a continuous, approach and the outcome of the limiting process had to be established. Moreover, the present method of solution shows how a 3-D analysis can indeed be developed to include also this continuous dependence on the angle θ and thus provide us with further insight on the construction of such 3-D solutions to transversely isotropic plates with more complicated flaw geometries.

It may further be noted that the macromechanical approach actually underestimates the value of the stresses at such regions. For example, if we examine the local geometry from a micromechanical point of view, e.g. at $\theta = 0°$ and for a [0°/90°] interface, one notices that the adjacent fiber of layer [90°] intersects the free surface of the hole boundary perpendicularly. The explicit 3-D solution for the stress field in such regions is also known. In particular, for a glass fiber embedded into an epoxy matrix the stress singularity is found to be 0.2489 (Folias, 1989, 1990) while for a carbon fiber embedded into an epoxy matrix is found to be 0.307 (Folias and Li, 1991). The former analysis assumes the fiber to be of an isotropic material while the latter assumes the fiber to be of a transversely isotropic material. Comparing these results with those of Fig. 4 it is clear that the stress singularity predicted by the macromechanical theory is indeed underestimated. Such information becomes essential for the proper estimation of the local damaged zone. This matter will be discussed further later on.
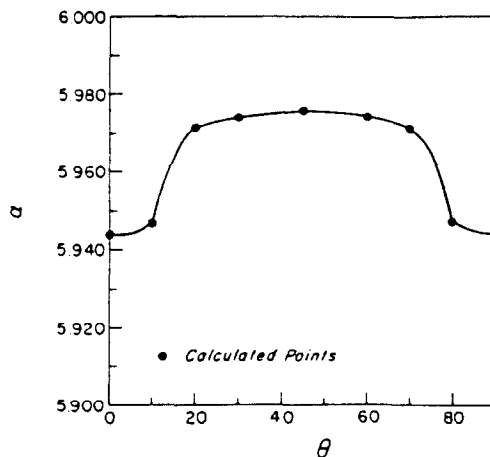
Fig. 6. Singularity strength for transversely isotropic laminae [0 90] based on Ericson *et al.* (1984) data.

In the case of a [0 /90] interface, the profile of the characteristic value α versus θ is symmetric with respect to the line $\theta = 45$. The same behavior was also obtained by Ericson *et al.* (1984) by using finite elements. The present results, however, exhibit a stronger singularity than that found in the above reference. The author attributes this to two factors. First the material constants were different and second it is rather difficult to obtain accurate results for the singularity strength based on finite element analyses. On the other hand, it is impressive indeed that Ericson *et al.* (1984) as well as Raju and Grews (1982) were able to recover the exact profile as a function of θ and the relative magnitude.

In order to make a proper comparison with the results of Ericson *et al.*, one should use the same material constants, C_{ij}, as they used. Computing, therefore, the C_{ij} values from their data (see Appendix B), our analysis gives the characteristic values depicted in Fig. 6. At $\theta = 45$, for example, $\alpha = 5.9755$ or $\alpha - 6 = 0.0245$. If we now compare this value with that found by Wang and Choi (1982), for $a \pm 45$ straight edge interface, i.e. $\alpha - 6 = 0.0255$, we see that the comparison is very good. The minor difference is probably due to the small variation of the C_{ij} values used depending as to how they are computed. Our results are based on the C_{ij} values shown in Appendix B. The results in the region between $20 < \theta < 70$ compare very well with those reported by Ericson *et al.* On the other hand, for $0 \leqslant \theta \leqslant 20$, our singularity strength is found to be slightly higher, and the characteristic bell-shaped profile is preserved.

Pagano and Pipes (1973) have shown that high-tensile σ_{zz} stresses are associated with decreased laminate strengths. This observation points to the importance of understanding the interlaminar stress behavior near free edges in laminates. It is now possible to compute the interlaminar stresses adjacent to the hole surface. In particular,

$$\sigma_{3i} \sim \rho^{\alpha-6} f_{3i}(\theta, \phi; C_{kl}, \tilde{C}_{mn}), \tag{62}$$

where the f_{3i} are rather long and complicated functions of the angles θ and ϕ and the material constants. The plots for σ_{zz}, τ_{rz}, $\tau_{\theta z}$, for a [0 /90] interface, are given in Fig. 7. Notice that the maximum σ_{zz} stress for a [0 /90] interface occurs† at $\theta = 23$. The result is in agreement with that found previously based on finite elements (Ericson *et al.*, 1984; Raju and Grews, 1982).

The reader may also note that all the stresses are normalized with respect to a function $C(\theta)$, which is negative, and may vary as one travels along the direction of θ. More specifically, the function represents the coefficient $\tilde{A}_3$. Through a separate analysis, which is to be valid across the thickness of the plate, it can be shown that the function is related to the magnitude and in-plane direction of the applied load σ_0. This part of the development

† The reader should also take into account the fact that $(6 - \alpha)$ is a maximum at $\theta^* = 45$ and that $C(\theta)$ is negative. The results are based on data given by eqn (61). Also, at $\theta = 0$, $C(\theta) \approx -1.0(h)^{\alpha-7}\sigma_0$.
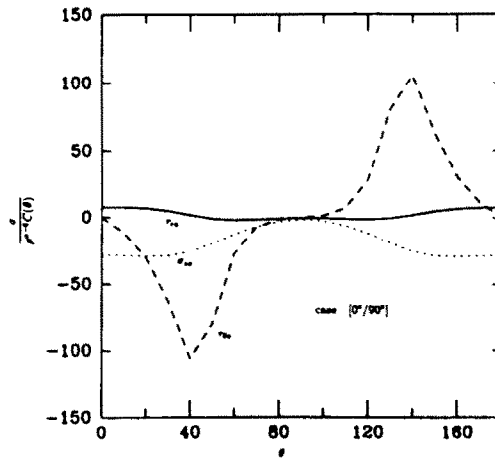
Fig. 7. Interlaminar stresses for a [0°/90°] interface.

is presently being completed, and the results will be reported in a follow up paper. In this second paper, the author also intends to couple the present macromechanical results with other newly derived results, which are based on 3-D micromechanical considerations, in order to predict local damage initiation. The present analysis, however, does provide us with the relative magnitudes of the interlaminar stresses (see Fig. 8). Moreover, the solution in its present form is very general, with the characteristics of the applied load being reflected only through the function $C(\theta)$.

The results show the shear stress τ_{rz} to be relatively low throughout. On the other hand, the normal stress σ_{zz} appears to be dominant in the range $-30° \leqslant \theta \leqslant 30°$, beyond which the shear stress $\tau_{\theta z}$ becomes the controlling stress, i.e. along $30° < \theta < 60°$, with its maximum occurring at $\theta = 45°$. A clearer plot for the stress σ_{zz} at the interface is given in Fig. 9. Finally, Fig. 10 depicts the jump which exists on the stress $\sigma_{\theta\theta}$ as one moves across the interface, i.e. at $\phi = 0^+$ and $\phi = 0^-$. The maximum difference occurs at $\theta = 0$ and is approximately 27%. In Figs 11 and 12 we compare the stress $\sigma_{\theta\theta}^{[0]}$ at $\phi = 0-$ and $\phi = -90°$, and $\sigma_{\theta\theta}^{[90]}$ at $\phi = 0+$ and $\phi = +90°$.

In view of the above, one may draw the following conclusions for a [0/90°] stacking sequence:

(a) In the vicinity of the interface there exists a boundary layer effect where the stress field changes rather abruptly.
(b) The risk of delamination initiation is highest at θ equal to $23°$.
(c) As one moves away from the plane of the interface, the stress concentration factor in layer [90°] decreases rapidly (see region $-20 < \theta < 20$ where debonding along fiber matrix interfaces is most likely to initiate).
(d) Substantial damage is expected in the region $-40° < \theta < 40°$.
(e) For the given set of material constants, C_{ij}, $\alpha - 6$ is maximum at $\theta^* = \theta_m^* \equiv (\beta/2)$.
(f) In general, the magnitude of the singularity strength depends on the material constants, C_{ij}, and on the fiber orientation of the two respective laminae.
(g) As one moves approximately one radius' distance away from the hole surface, the s.c.f. (stress concentration factor) is expected to decrease to within 10% of the value of the corresponding case of a plate without a hole (Folias and Wang, 1990: isotropic case).

6. DISCUSSION

Delamination at free edges has been a problem of significant concern in the design of advanced fiber composites. The separation of the laminae, caused by high local interlaminar stresses and low strength along the laminae interface, may result in ineffective load transfer, reduction in stiffness and ultimately loss of structural integrity. In this study, the problem has been investigated by treating each lamina as a homogeneous, transversely isotropic,
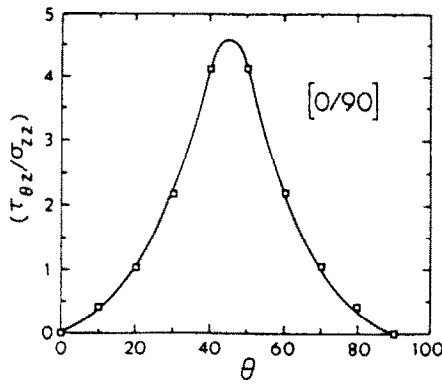
Fig. 8. Interlaminar shear stress ratio for a [0°/90°] interface.

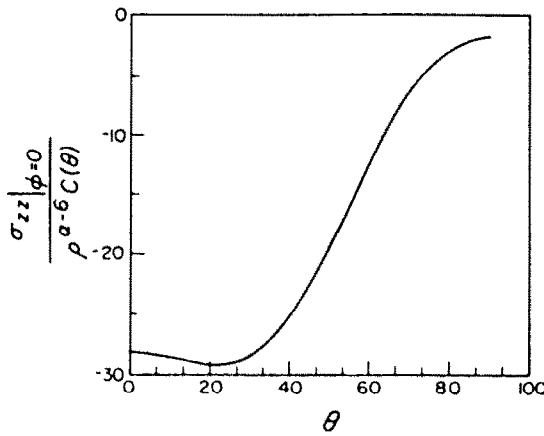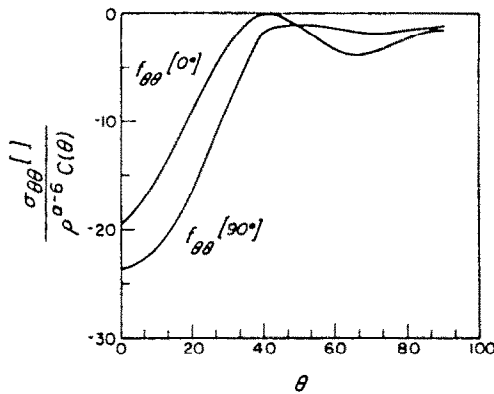Fig. 9. The interlaminar stress σ_{ii} versus θ.

Fig. 10. The stress concentration factor for $\phi = 0^+$ and 0^-.

material. Thus the micromechanic effects of fiber size are not included, although a few of these effects, e.g. when a fiber meets a free surface, have been reported separately by Folias (1989, 1990).

The analytical investigation of the 3-D stress field adjacent to the hole and in the vicinity of the interfaces of two laminae of [0°/90°], and [0°/45°], and other fiber orientation, shows the stresses to be singular, $\sigma_{ij} \sim \rho^{\alpha-6}$. In general, the singularity exponent depends on the material properties, the corresponding fiber orientations as well as the angle of sweep. The results provide us with better insight for the proper understanding of inter-laminar stresses and the effect which they have on the mechanism of failure. For example, for isotropic laminae the stress singularity is a rather weak singularity (<0.33), while in
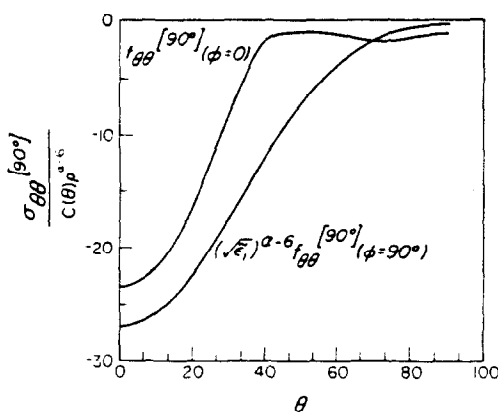
Fig. 11. The stress $\sigma_{\theta\theta}^{[90]}$ for $\phi = 0^+$ and $\phi = 90^\circ$.
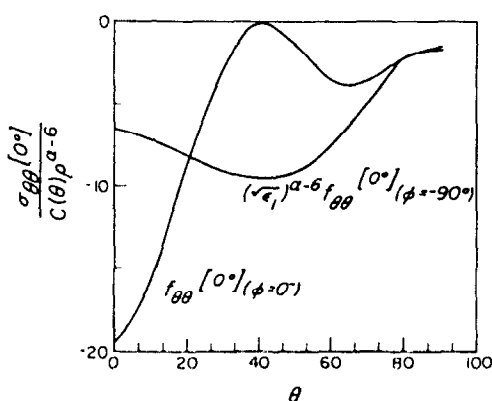
Fig. 12. The stress $\sigma_{\theta\theta}^{[0]}$ for $\phi = 0$ and $\phi = -90^\circ$.

transversely isotropic laminae it can be of a much higher order (<0.99), suggesting, therefore, a greater influence in the damage process.

Pipes *et al.* (1973) and Pagano (1974) postulated that throughout the thickness it is the stress σ_{zz} which is the main cause of delamination for polymer-based structural composites. This observation was based on experimental as well as analytical evidence for laminates with different stacking sequences. Our analytical results are consistent with this observation particularly in the region where θ is small. Alternatively, for larger values of θ the shear stress $\tau_{\theta z}$ plays a much more dominant role on interlaminar failures. Moreover, in the case of a $[0^\circ/90^\circ]$ interface delamination is most likely to take place at $\theta = 23^\circ$. The strain energy release rate may now be used in conjunction with the local stress field to predict delamination failures. This matter is presently under investigation.

Finally, one may conclude that it is possible to reduce the likelihood of the delamination mode of failure and thereby increase the laminate strength. This can be accomplished by carefully considering the effects of the singularity curves, the stress curves, the load direction and the individual fiber orientations at each interface. Moreover, in future applications it may be possible to choose the material constants C_{ij} so that the coefficients of the singular terms of the interlaminar stresses vanish.

REFERENCES

Bakis, C. E. and Stinchcomb, W. W. (1986). Response of thick, notched laminates subjected to tension-compression cyclic loads. *ASTM STP* 907, 314–334.

Daniel, I. M., Rowlands, R. E. and Whiteside, J. B. (1974). Effects of material and stacking sequence on behavior of composite plates with holes. *Exp. Mech.* **14**(1), 1-9.

Ericson, K., Persson, M., Carlsson, L. and Gustavsson, A. (1984). On the prediction of the initiation of delamination in a [0 90]s laminate with a circular hole. *J. Compos. Mater.* **18**, 495 506.

Folias, E. S. (1988). On the interlaminar stresses of a composite plate around the neighborhood of a hole. *Int. J. Solids Structures* **25**(10), 1193 1200.

Folias, E. S. (1989). On the stress singularities at the intersection of a cylindrical inclusion with the free surface of a plate. *Int. J. Fract.* **39**, 25 34.

Folias, E. S. (In press). On the prediction of failure at a fiber matrix interface in a composite subjected to a transverse tensile load. *J. Compos. Mater.*

Folias, E. S. and Reuter, W. G. (1990). On the equilibrium of a linear elastic layer. *Comput. Mech.* **5**(6), 459 468.

Folias, E. S. and Wang, J. J. (1990). On the three-dimensional stress field around a circular hole in a plate of arbitrary thickness. *Int. J. Comput. Mech.* **6**(5), 379 391.

Knight, M. (1982). Three-dimensional elastic moduli of graphite epoxy composites. *J. Compos. Mater.* **16**, 153 161.

Li, P. and Folias, E. S. (In press). The 3D stress field of a carbon fiber embedded into an epoxy matrix and intersecting a free surface. *J. Mech. Mater.*

Pagano, N. J. and Pipes, R. B. (1973). Some observations on the interlaminar strength of composite materials. *Int. J. Mech. Sci.* **15**, 679 686.

Pagano, N. J. (1974). On the calculation of interlaminar normal stress in composite laminates. *J. Compos. Mater.* **8**, 89 95.

Pipes, R. B., Kaminski, B. E. and Pagano, N. T. (1973). Influence of the free edge upon the strength of angle-ply laminates. *ASTM STP* **521**, 218 226.

Raju, I. S. and Crews, J. H. (1982). Three-dimensional analysis of [0 90]s and [90 0]s laminates with a central circular hole. *Compos. Technol. Rev.* **4**, 116 127.

Rybicki, E. F. and Schmueser, D. W. (1978). Effect of stacking sequence and lay-up angle on free edge stresses around a hole in a laminated plate under tension. *J. Compos. Mater.* **12**, 300 313.

Wang, S. S. and Choi, I. (1982). Boundary-layer effects in composite laminates: Part I Free-edge stress singularities. *J. Appl. Mech.* **49**, 541 560.

APPENDIX A

Verification of solution (eqn (36))

Use local coordinates defined by eqns (34) and (35) to write eqn (18) in the form

$$\nabla_1^2 \nabla_2^2 \nabla_1^2 H = \nabla_1^2 \nabla_2^2 \nabla_1^2 H = 0$$

define

$$\nabla_1^2 H_1 = 0$$

and assume

$$H_1 = \rho_1^{\chi - 4} F_1(\phi)$$

which implies

$$F_1 = A_1 \cos(\chi - 4)\phi_1 + B_1 \sin(\chi - 4)\phi_1$$

where

$$\rho_1 = \sqrt{(r-a)^2 + \frac{(h-z)^2}{c_1}}$$

$$\phi_1 = \tan^{-1}\left(\frac{(h-z)\sqrt{c_1}}{r-a}\right).$$

Thus

$$H_1 = \nabla_2^2 \nabla_1^2 H = \nabla_2^2 H_2 = \rho_1^{\chi - 4} F_1(\phi_1)$$

$$= \rho_2^{\chi - 4}\left(\frac{\rho_1}{\rho_2}\right)^{\chi - 4} F_1(\phi_1)$$

where

$$\frac{\rho_3}{\rho_2} = \sqrt{\frac{(r-a)^2 + \dfrac{(h-z)^2}{\epsilon_1}}{(r-a)^2 + \dfrac{(h-z)^2}{\epsilon_2}}}$$

$$= \sqrt{\frac{1 + \dfrac{\epsilon_2}{\epsilon_3}\dfrac{(h-z)^2}{\epsilon_2(r-a)^2}}{1 + \dfrac{(h-z)^2}{\epsilon_2(r-a)^2}}}$$

$$= \sqrt{\frac{1 + \dfrac{\epsilon_2}{\epsilon_3}\tan^2\phi_2}{1 + \tan^2\phi_2}},$$

and

$$\tan\phi_3 = \frac{(h-z)}{\sqrt{\epsilon_3}(r-a)} = \sqrt{\frac{\epsilon_2}{\epsilon_3}}\frac{1}{\sqrt{\epsilon_2}}\frac{h-z}{r-a}$$

$$\Rightarrow \phi_3 = \tan^{-1}\left(\sqrt{\frac{\epsilon_2}{\epsilon_3}}\tan\phi_2\right).$$

etc. for V_2^i and V_1^i.

Solution of system (1) (3)
   Let

$$u = \frac{\partial U}{\partial x} = \sin\theta\,\frac{\partial U}{\partial(r-a)} + \frac{\cos\theta}{r}\frac{\partial U}{\partial\theta}$$

$$v = \frac{\partial V}{\partial y} = \cos\theta\,\frac{\partial V}{\partial(r-a)} - \frac{\sin\theta}{r}\frac{\partial V}{\partial\theta}$$

$$w = \frac{\partial W}{\partial z}.$$

Such a substitution eliminates the cross type of derivatives. Then utilize cylindrical coordinates and use the assumption $(r-a)/a \ll 1$. By direct substitution, one can then show that the simplified governing equation is indeed satisfied provided that function H satisfies eqn (18).

APPENDIX B

From Ericson *et al.* (1984) data:

$$E_{11} = 138\,\text{GPa} \qquad E_{22} = E_{33} = 14.5\,\text{GPa}$$

$$G_{12} = G_{13} = G_{23} = 5.9\,\text{GPa}$$

$$\nu_{12} = \nu_{13} = \nu_{23} = 0.21,$$

we compute:

$$C_{11} = 139.6381$$
$$C_{12} = 3.9002$$
$$C_{13} = 3.9002$$
$$C_{22} = 15.2779$$
$$C_{23} = 3.2944$$
$$C_{33} = 15.2779$$
$$C_{44} = C_{55} = C_{66} = 5.9;$$

in view of which our program then gives:

θ	χ
0.1	5.9440
10	5.9469
15	5.9698
20	5.9714
30	5.9739
45	5.9755